

<http://darcycenter.org>

Peer reviewed:

Yes, Vadose Zone J. 18:180133. doi:10.2136/vzj2018.07.0133

Title:

The Effect of Dynamic Capillarity in Modeling Saturation Overshoot during Infiltration

Author:

Luwen Zhuang¹, C.J. van Duijn^{1,2}, and S. Majid Hassanizadeh¹

1. Department of Earth Sciences, Utrecht University, P.O. Box 80021, 3508TA Utrecht, The Netherlands
2. Department of Mechanical Engineering, Eindhoven University of Technology, P.O. Box 513, 5600 MB Eindhoven, The Netherlands

Publication date:

2-2019

Copyright information:

Copyright and moral rights for the publications made accessible in the public portal are retained by the authors and/or other copyright owners and it is a condition of accessing publications that users recognise and abide by the legal requirements associated with these rights. Users may download and print one copy of any publication from the public portal for the purpose of private study or research. You may not further distribute the material or use it for any profit-making activity or commercial gain. You may freely distribute the URL identifying the publication in the public portal.

Original Research

Core Ideas

- We provide detailed analysis of various forms of the dynamic capillarity coefficient.
- We focus on the region of saturation overshoot at larger saturation.
- The results are evaluated with the aid of experimental observations.

L. Zhuang, C.J. van Duijn, and S.M. Hassanizadeh, Dep. of Earth Sciences, Utrecht Univ., Budapestlaan 4, 3584 CD Utrecht, The Netherlands; C.J. van Duijn, Dep. of Mechanical Engineering, Eindhoven Univ. of Technology, P.O. Box 513, 5600 MB, Eindhoven, The Netherlands; S.M. Hassanizadeh, Soil and Groundwater Systems, Deltares, Princetonlaan 6, 3584 CB Utrecht, The Netherlands. *Corresponding author (luwen.zhuang@gmail.com).

Received 10 July 2018.
Accepted 3 Oct. 2018.

Citation: Zhuang, L., C.J. van Duijn, and S.M. Hassanizadeh. 2019. The effect of dynamic capillarity in modeling saturation overshoot during infiltration. *Vadose Zone J.* 18:180133. doi:10.2136/vzj2018.07.0133

© Soil Science Society of America.
This is an open access article distributed under the CC BY-NC-ND license (<http://creativecommons.org/licenses/by-nc-nd/4.0/>).

The Effect of Dynamic Capillarity in Modeling Saturation Overshoot during Infiltration

Luwen Zhuang,* C.J. van Duijn, and S. Majid Hassanizadeh

Gravity-driven fingering has been observed during downward infiltration of water into dry sand. Moreover, the water saturation profile within each finger is non-monotonic, with a saturation overshoot at the finger tip. As reported in the literature, these effects can be simulated by an extended form of the Richards equation, where a dynamic capillarity term is included. The coefficient of proportionality is called the dynamic capillarity coefficient. The dynamic capillarity coefficient may depend on saturation. However, there is no consensus on the form of this dependence. We provide a detailed traveling wave analysis of four distinctly different functional forms of the dynamic capillarity coefficient. In some forms, the coefficient increases with increasing saturation, and in some forms, it decreases. For each form, we have found an explicit expression for the maximum value of saturation in the overshoot region. In current formulations of dynamic capillarity, if the value of the capillarity coefficient is large, the value of saturation in the overshoot region may exceed unity, which is obviously nonphysical. So, we have been able to ensure boundedness of saturation regardless of the value of the dynamic capillarity coefficient by extending the capillary pressure–saturation relationship. Finally, we provide a qualitative comparison of the results of traveling wave analysis with experimental observations.

Abbreviations: TW, traveling wave.

Traditionally, in two-phase flow systems, the difference between the non-wetting-phase pressure and the wetting-phase pressure is assumed to be equivalent to the capillary pressure. The relationship between capillary pressure and water saturation is fundamental for the characterization of unsaturated flow in porous media. Traditionally, this relationship is assumed to be independent of flow rates. However, it has been reported that the relation between the fluid pressure difference and water saturation during dynamic processes differs from that under static conditions (see e.g., Topp and Peters, 1967; Smiles et al., 1971; Vachaud and Thony, 1971; Elzeftawy and Mansell, 1975; Stauffer, 1978; Wildenschild et al., 2001; O'Carroll et al., 2005). Stauffer (1978) proposed to define a dynamic capillary pressure in addition to the standard static capillary pressure. Through experimental studies, he found that the difference between dynamic and static capillary pressure depends linearly on the temporal rate of change of saturation.

Following Hassanizadeh and Gray (1990) and Kalaydjian (1987), we choose a different conceptual approach. According to this approach, there is only one capillary pressure and that is the one measured under quasi-static conditions. What is measured under dynamic conditions is not capillary pressure but the difference between the two fluid pressures. Based on a thermodynamic approach, they showed that the difference in fluid phase pressures under dynamic conditions is not just equal to the standard capillary pressure but includes a dynamic term dependent on the temporal rate of saturation change. A linearized approximation was proposed by Hassanizadeh and Gray (1993) as

$$p^n - p^w = p^{cw} - \tau \frac{\partial S^w}{\partial t} \quad [1]$$

where p^n [$\text{ML}^{-1} \text{T}^2$] and p^w [$\text{ML}^{-1} \text{T}^2$] are non-wetting- and wetting-phase pressures, respectively, and p^{cw} [$\text{ML}^{-1} \text{T}^2$] is the capillary pressure. It is obtained as the difference between

non-wetting and wetting pressures under quasi-static conditions. Further, S^w (dimensionless) is the wetting-phase saturation, and τ [$M L^{-1} T$] is a nonequilibrium (or dynamic) capillarity coefficient. Recent studies have suggested that the dynamic coefficient τ varies with saturation (Dahle et al., 2005; Manthey et al., 2005; Camps-Roach et al., 2010; Joekar-Niasar et al., 2010; Goel and O'Carroll, 2011; Bottero et al., 2011). Comprehensive reviews on experimental and numerical research related to the effect of dynamic capillarity were given by Hassanizadeh et al. (2002), Diamantopoulos and Durner (2012), and Joekar-Niasar and Hassanizadeh (2012).

A number of studies have quantified the value of the dynamic capillarity coefficient τ at different saturation values, but the functional relationship between saturation and τ is still unclear. Different studies have produced different or even contradictory trends. In laboratory experiments with sand columns, Oung et al. (2005) and Bottero et al. (2011) found that the variation of τ with saturation was not significant. However, some other experimental studies have shown that the value of τ generally decreases with increasing saturation. Rapid primary drainage experiments done in a water-tetrachloroethylene (PCE) porous system (Hassanizadeh et al., 2004; Bottero et al., 2006; Das and Mirzaei, 2012) and in an air-water porous system (Sakaki et al., 2010; Goel and O'Carroll, 2011) have shown that τ varies as a logarithmic function of the inverse of saturation in the range $0.4 < S^w < 1$. Further, O'Carroll et al. (2005, 2010) determined the value of τ through inverse modeling of multistep outflow PCE-water experiments and proposed a linear relationship with the inverse of saturation. A similar decreasing τ - S^w relationship has been reported in various numerical studies based on both pore-scale (Dahle et al., 2005; Gielen, 2007; Joekar-Niasar and Hassanizadeh, 2011) and continuum-scale simulations (Manthey et al., 2005; Berentsen et al., 2006; Mirzaei and Das, 2007; Fučík et al., 2010). A totally opposite trend was found by Camps-Roach et al. (2010) and Sakaki et al. (2010), who did primary drainage and main imbibition experiments, respectively. They reported that τ increases with increasing saturation.

Addition of the dynamic capillarity Eq. [1] to the standard equations for two-phase flow (or unsaturated flow) leads to a totally different mathematical model. While standard equations are known to be unconditionally stable and give monotonic saturation profiles (Egorov et al., 2002), the dynamic capillarity model has shown to be conditionally unstable and may result in non-monotonic saturation profiles (Egorov et al., 2002; van Duijn et al., 2004). There are only a few works on mathematical analysis of the dynamic capillarity effect. Moreover, most of them have considered a constant value for τ (see, e.g., Cuesta and Hulshof, 2003; van Duijn et al., 2007, 2013; Rätz and Schweizer, 2014; Cao and Pop, 2016; Zhang and Zegeling, 2017). Nieber et al. (2005) and Sander et al. (2008) analyzed unsaturated flow equations including the dynamic capillarity term for a non-monotonic τ - S^w relationship, which goes to infinity when S^w is close to 0 and 1.

As explained above, the form of the τ - S^w function is not clearly determined yet. The solution of governing equations will certainly be affected by such a functional relationship. Therefore,

it would be extremely useful to know how the solution of equations will change with the various forms of the dependence of τ on saturation. This will be helpful in analyzing experimental results and finding the correct form of the τ - S^w relationship.

In this work, we analyze and discuss the effect of the dynamic capillarity coefficient on saturation (overshoot) in the unsaturated flow model. We consider as examples four different relationships between τ and S^w , and show how saturation is affected by them. The current formulation of the dynamic capillarity model does not guarantee that the saturation overshoot will not exceed unity for large values of τ . Therefore, we extended the capillary pressure-saturation relationship to ensure that the saturation value does not exceed unity regardless of the τ value. Also, we have found an explicit expression for the maximum value of saturation in the overshoot region. Finally, we evaluate the results of the traveling wave analysis with the aid of experimental observations. We emphasize that our aim is not to simulate specific experiments. To do so, more information and additional effects have to be included, such as hysteresis in capillary and relative permeability.

Experimental Observations

Gravity-driven fingering in unsaturated porous media has been observed experimentally and simulated numerically in many studies (e.g., Baker and Hillel, 1990; Wang et al., 2004; DiCarlo, 2007; Chapwanya and Stockie, 2010). Comprehensive reviews of theories, models, and experiments have been performed by DiCarlo (2013) and Xiong (2014).

Among these, several experiments have reported that a characteristic saturation overshoot occurred at the tip of each finger (DiCarlo, 2004; Fritz, 2012), as well as non-monotonic water pressure profiles (Stonestrom and Akstin, 1994; DiCarlo, 2007). Here we show two sets of typical experimental results during gravity-driven fingering flow.

DiCarlo (2004) performed a series of one-dimensional water infiltration experiments with dry clean sand ($S^w \approx 0$). The experiments were done at six different water flow rates. Water saturation distributions along the domain were measured using the light transmission method. Figure 1 shows the water saturation profiles obtained at different water flow rates. As shown, the saturation profiles are monotonic at the highest (11.8 cm/min) and the lowest (8×10^{-4} cm/min) inflow rates, while there exists saturation overshoot for all other inflow rates. The overshoot becomes higher and wider with increasing inflow rate, except for the highest inflow rate.

Fritz (2012) conducted gravity-driven infiltration experiments under different but uniform initial saturations. Saturation was measured at 20 cm from the inlet during all experiments. Figure 2 presents saturation breakthrough curves obtained under three different initial saturations for the same inflow rate (0.26 cm/min). At higher values of initial saturation, the overshoot height decreased and even vanished for the largest initial saturation. Obviously, both initial and boundary conditions influence the shape of saturation overshoot.

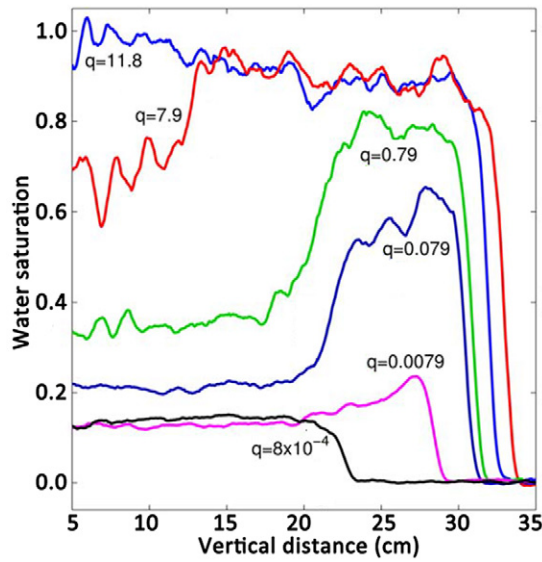


Fig. 1. Saturation profiles during infiltration for six different inflow rates q (cm/min) (DiCarlo, 2013).

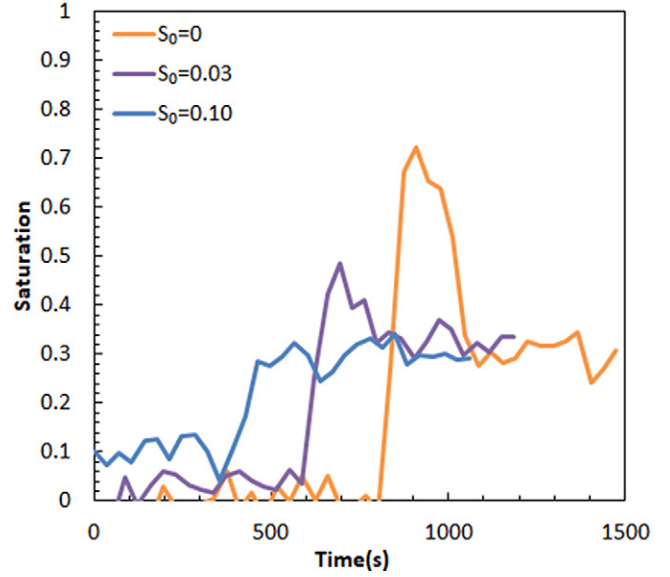


Fig. 2. Saturation breakthrough curve at 20 cm at three different initial saturations with a flow rate of 0.26 cm/min (Fritz, 2012).

In the following, we first report on analytical results of the traveling wave solutions concerning different forms of the dynamic capillarity coefficient. Then, we show calculations with different initial and boundary conditions, using the typical parameter values for sandy soil (i.e., reported by DiCarlo [2004] and Fritz [2012]). The parameters used in the calculations are summarized in Table 1.

Governing Equations

Consider a vertical column filled with homogeneous soil, having porosity ϕ (dimensionless) and intrinsic permeability k [L^2]. The one-dimensional continuity equation for the water phase is

$$\phi \frac{\partial S^w}{\partial t} + \frac{\partial}{\partial x} \left[-\frac{k^{rw}(S^w)k}{\mu} \left(\frac{\partial p^w}{\partial x} - \rho^w g \right) \right] = 0 \quad [2]$$

with

$$p^a - p^w = p^{cw}(S^w) \quad [3]$$

where p^a [$M L^{-1} T^{-2}$], $k^{rw}(S^w)$ (dimensionless), p^w [$M L^{-1} T^{-2}$], and ρ^w [$M L^{-3}$] denote air pressure, relative permeability, water pressure, and water density, respectively. Further, μ [$M L^{-1} T$] is water viscosity, x [L] is the vertical coordinate (with positive direction pointing downward), t [T] is time, g [$L T^{-2}$] is the gravitational constant, and ϕ (dimensionless) is porosity. In Eq. [3], $p^{cw}(S^w)$ [$M L^{-1} T^{-2}$] is the capillary pressure, defined as the difference between air pressure and water pressure under equilibrium conditions.

In this study, we include the dynamic capillarity effect and replace Eq. [3] with Eq. [1]. In an air–water system, the result is

$$p^a - p^w = p^{cw}(S^w) - \tau^w(S^w) \frac{\partial S^w}{\partial t} \quad [4]$$

where $\tau^w(S^w)$ [$M L^{-1} T$] is the dynamic capillarity coefficient. It is a given function of the water saturation, whose influence we wish to study.

The air pressure is considered as a constant reference pressure. Hence it can be eliminated from Eq. [4] by redefining the water pressure p^w . The van Genuchten–Mualem model (van Genuchten, 1980) is used for the relationships describing capillary pressure and relative permeability in terms of water saturation:

$$p^{cw}(S^w) = \frac{1}{\alpha} (S_e^{-1/m} - 1)^{1/n} \quad [5]$$

$$k^{rw}(S^w) = S_e^{0.5} \left[1 - (1 - S_e^{1/m})^m \right]^2 \quad [6]$$

$$S_e = \frac{S^w}{1 - S_r^a} = \frac{S^w}{S_m} \quad [7]$$

where S_e (dimensionless), S_a^r (dimensionless), and $S_m = 1 - S_r^a$ (dimensionless) denote effective water saturation, residual air

Table 1. The parameter values used in the calculations.

Parameters	Value
Porosity (ϕ)	0.4
Water density (ρ^w), kg/m ³	1×10^3
Water viscosity (μ^w), Pa s	1×10^{-3}
Primary imbibition retention exponent n	2.58
Primary imbibition retention parameter α , 1/Pa	8.6×10^{-3}
Residual air saturation (S_a^r)	0.05
Intrinsic permeability (k), m ²	6.43×10^{-10}
Inflow water flux (q_T), cm/min	0.26

saturation, and maximum water saturation, respectively; α [L^{-1}] and n (dimensionless) are fitting parameters, and $m = 1 - 1/n$. We hint that because this study focuses on the effect of the saturation-dependent coefficient $\tau^w = \tau^w(S^w)$, we disregard any hysteresis in capillary pressure and relative permeability. For $p^{cw}(S^w)$ in Eq. [4], we use the capillary pressure–saturation relation for primary imbibition.

Nieber et al. (2005) proposed to include a pressure dependence in τ as well: in our notation $\tau = \tau(S^w, p^w)$. However, since the current study uses the analytical results of van Duijn et al. (2018), where $\tau = \tau(S^w)$ only, we shall restrict ourselves to this case as well.

The problem that we study describes the injection of water into an infinitely long column $\{0 < x < \infty\}$. This column is initially filled with water and air such that the water saturation has a (small) constant value: $S^w(x, 0) = S_B$ for all $x > 0$. At the top ($x = 0$), water is injected at the constant rate q_T [$L T^{-1}$]. Using Darcy's law, the injection rate q_T can be converted into a boundary saturation $S^w(0, t) = S_T$ satisfying

$$q_T \approx \frac{\rho^w g k}{\mu} k^{rw}(S_T) \quad [8]$$

This relation is expected to hold fairly soon after the injection starts.

For numerical purposes we truncate the column at a finite, but large, depth $x = L$. There we prescribe $S(L, t) = S_B$ for all $t > 0$. The running terms t in Eq. [2] and the depth L are chosen so that the water distribution in the column is not influenced by the boundary condition at $x = L$.

◆ Nondimensionalization of Equations

To discuss and compare the results of van Duijn et al. (2018) in terms of Eq. [2] and [4] and the boundary and initial conditions, we first need to make the problem dimensionless. For this purpose, characteristic values for length (x_R), time (t_R), pressure (p_R), water flux (q_R), and dynamic capillarity (τ_R) are introduced. With these values, we consider the dimensionless variables

$$t_D = \frac{t}{t_R}, \quad x_D = \frac{x}{x_R}, \quad u = \frac{p^a - p^w}{p_R}, \quad p_D^c(S^w) = \frac{p^{cw}(S^w)}{p_R}, \quad q_D = \frac{q^w}{q_R}$$

(dimensionless water flux), and (dimensionless capillarity)

$$\tau_D(S^w) = \frac{\tau^w(S^w)}{\tau_R} \quad [9]$$

where u denotes the dimensionless pressure difference.

Substituting these scaled variables into Eq. [2] and [4] gives

$$\frac{\partial S^w}{\partial t_D} + \frac{\rho^w g k t_R}{\phi \mu x_R} \frac{\partial}{\partial x_D} \left[k^{rw}(S^w) \left(\frac{p_R}{\rho^w g x_R} \frac{\partial u}{\partial x_D} + 1 \right) \right] = 0 \quad [10a]$$

$$u = p_D^c(S^w) - \frac{\tau_R}{p_R t_R} \tau_D(S^w) \frac{\partial S^w}{\partial t_D} \quad [10b]$$

Balancing terms in Eq. [10a] gives

$$\frac{\rho^w g k t_R}{\phi \mu x_R} = 1 \quad \text{and} \quad \frac{p_R}{\rho^w g x_R} = 1 \quad [11]$$

Because we use Eq. [5] for p^{cw} , a natural choice for the characteristic pressure is $p_R = 1/\alpha$ (Pa). Using this in Eq. [11] yields

$$x_R = \frac{1}{\rho^w g \alpha} \quad \text{and} \quad t_R = \frac{\phi \mu}{\alpha (\rho^w g)^2 k} \quad [12]$$

Using these expressions in Eq. [10] yields

$$\frac{\partial S^w}{\partial t_D} + \frac{\partial}{\partial x_D} \left[k^{rw}(S^w) \left(\frac{\partial u}{\partial x_D} + 1 \right) \right] = 0 \quad [13a]$$

$$u = p_D^c(S^w) - \lambda \tau_D(S^w) \frac{\partial S^w}{\partial t_D} \quad [13b]$$

where

$$\lambda = \frac{(\alpha \rho^w g)^2 k}{\phi} \tau_R \quad [13c]$$

where λ denotes the dimensionless capillarity coefficient. Note that the dimensional τ_R refers to the dynamic capillarity coefficient measured in experiments. Dependent on the setting, it takes values in the range 10^4 to 10^7 Pa s (Hassanizadeh et al., 2002).

The water flux in the column is given by Darcy's law:

$$q^w = - \frac{k^{rw}(S^w) k}{\mu} \left(\frac{\partial p^w}{\partial x} - \rho^w g \right) \quad [14]$$

Because its value is prescribed at the top, i.e., $q^w(0, t) = q_T$, the natural scaling is $q_R = q_T$. Now, making Eq. [14] dimensionless gives

$$q_D = \frac{\rho^w g k}{\mu q_T} k^{rw}(S^w) \left(\frac{\partial u}{\partial x_D} + 1 \right)$$

This results in the boundary condition

$$k^{rw}(S^w) \left(\frac{\partial u}{\partial x_D} + 1 \right) \Big|_{x_D=0} = Q_T \quad [15]$$

where

$$Q_T = \frac{\mu q_T}{\rho^w g k} \quad [16]$$

Dropping the subscript D from the notation and writing $S = S^w$ and $k(S) = k^{rw}(S^w)$, we arrive at the following dimensionless formulation:

Find $0 < S \leq S_m$ such that

$$\frac{\partial S}{\partial t} + \frac{\partial}{\partial x} \left[k(S) \left(\frac{\partial u}{\partial x} + 1 \right) \right] = 0 \quad [17a]$$

$$u = p^c(S) - \lambda \tau(S) \frac{\partial S}{\partial t} \quad [17b]$$

for $x > 0$ and $t > 0$, subject to the boundary condition

$$k(S) \left(\frac{\partial u}{\partial x} + 1 \right) \Big|_{x=0} = Q_T \quad \text{for } t > 0 \quad [17c]$$

and the initial condition

$$S(x,0) = S_B \text{ for } x > 0 \quad [17d]$$

where p^c is the scaled version of Eq. [5] and $k(S)$ is given by Eq. [6].

After some time, the saturation at the top of the column becomes constant in time. Its value, $S = S_T$, follows from the dimensionless form of Eq. [8]:

$$k(S_T) = Q_T \quad [18]$$

where k is given by Eq. [6]. Later, when discussing traveling wave solutions of Eq. [17a–17b], we use S_T as the upstream limiting value. The initial value S_B is the downstream limiting value.

It is known (see, e.g., Cuesta et al. [2000] or Nieber et al. [2005]) that due to the dynamic term in Eq. [17b], the value of the water saturation is not constrained. Large λ values may lead to large saturation overshoot. To prevent the non-physical behavior where $S > S_m$, we need to extend the capillary pressure at $S = S_m$ in a way that allows for negative u values (or $p^w > p^a$). Mathematically, this is achieved by considering a set-valued capillary pressure at $S = S_m$:

$$p^c(S) = \begin{cases} (S_e^{-1/m} - 1)^{1/n} & \text{for } S < S_m \\ (-\infty, 0] & \text{at } S = S_m \end{cases} \quad [19]$$

Its dimensionless form is $p^c(S) = p^{cw}(S)/p_R$ (see Eq. [9]). As we demonstrate below, this extension ensures that, no matter how large the capillarity coefficient $\tau(S)$, the resulting saturation cannot exceed $S = S_m$ (see Fig. 3). Throughout this study, we use Eq. [19] for p^c in Eq. [17b]. Suppose $S = S_m$ in a region R as sketched in Fig. 4. Then clearly $\partial S/\partial t = 0$ in R . Hence from Eq. [17b], $u \leq 0$ in R and from Eq. [17a], $\partial^2 u/\partial x^2 = 0$ in R . This means that in regions where the saturation reaches its maximal value $S = S_m$, the pressure is hydrostatic.

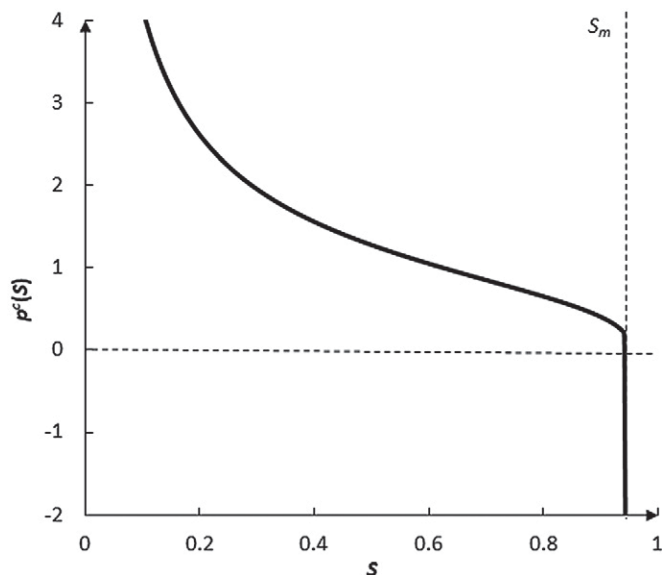


Fig. 3. Graph of extended capillary pressure based on Eq. [19].

The expression for λ is given by Eq. [13c]. Its value is determined by the physical and experimental constants involved. We shall consider it as a free parameter.

Concerning the capillarity function $\tau(S)$, we assume that it is positive and continuous in the interval $0 \leq S < S_m$ and that it may have a singularity at $S = S_m$ in the sense that

$$\lim_{S \rightarrow S_m} \tau(S) = \infty$$

In fact (see van Duijn et al., 2018), we shall distinguish between two classes of possible $\tau(S)$ functions:

$$\int_0^{S_m} \tau(S) dS < \infty \quad (\text{Class A}) \quad [20a]$$

$$\int_0^{S_m} \tau(S) dS = \infty \quad (\text{Class B}) \quad [20b]$$

Example: Let $f(S) = (S_m - S)^\omega$ for $0 < S < S_m$ with $-\infty < \omega < +\infty$. Then

$$\int_0^{S_m} f(S) dS = \begin{cases} \frac{1}{1+\omega} S_m^{1+\omega} < \infty & \text{if } \omega > -1 \\ \infty & \text{if } \omega \leq -1 \end{cases}$$

where f is integrable (Class A) if $\omega > -1$ (although $f(S)$ has singular behavior as $S \rightarrow S_m$ if $-1 < \omega < 0$) and f is non-integrable (Class B) if $\omega \leq -1$.

The four τ - S relations are given in Table 2 and plotted in Fig. 5. Example $\tau_2(S)$, where τ_2 decreases with S , corresponds to experimental results found in many references (see, e.g., Hassanizadeh et al., 2004; Mantney et al., 2005; Bottero et al., 2006; Joekar-Niasar and Hassanizadeh, 2011; Das and Mirzaei, 2012). Examples $\tau_3(S)$ and $\tau_4(S)$ follow trends found in Camps-Roach et al. (2010) and Sakaki et al. (2010). Clearly τ_1, τ_2 , and τ_3 belong to Class A, while τ_4 belongs to Class B.

Numerical Solution of Flow Equations

Here we present the numerical solution of the dimensionless problem Eq. [17], with p^c given by the extended version Eq. [19]. The parameters involved are the dimensionless capillarity constant λ and the dimensionless inflow rate Q_T . The values of the underlying relevant physical quantities are given in Table 1. Those values yield the dimensionless injection rate (see Eq. [16]):

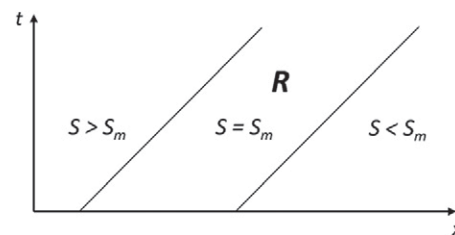


Fig. 4. Sketch of region R where saturation $S = S_m$, the maximum water saturation.

Table 2. Different expressions for the capillarity function $\tau(S)$.

Dynamic capillarity function	Expression†
$\tau_1(S)$ (constant)	1
$\tau_2(S)$ (decreasing)	$1 - S/S_m$
$\tau_3(S)$ (increasing)	S/S_m
$\tau_4(S)$ (increasing and non-integrable)	$1/(1 - S/S_m)$

† S , saturation; S_m , maximum saturation.

$$Q_T = 6.7 \times 10^{-3} \quad [21]$$

This value of Q_T , based on Eq. [6] and [18], results in an upstream saturation S_T value of 0.33. The values in Table 1 were taken from experiments performed by Fritz (2012). Although several other inflow rates were considered in the experiments, we regard the values from Table 1 as our base case.

We show the results of two sets of numerical experiments: one where $\tau(S) = 1$ and one where $\tau(S) = 1/(1 - S/S_m)$. This corresponds to Cases 1 and 4 from Table 3. For each chosen $\tau(S)$, we show numerical results for different values of λ : $\lambda = 10$, $\lambda = 50$, and $\lambda = 100$. In the experiments of Fritz (2012), the sand column was initially (almost) dry. In the numerical experiments, we took $S_B = 0.01$ to avoid singular behavior of the capillary pressure. To avoid the multi-valuedness in Eq. [19], we replaced this expression in the computations by the approximation

$$p^c(S) = \begin{cases} (S e^{-1/m} - 1)^{1/n} & \text{for } S \leq S_m - \sigma \\ \frac{1}{\epsilon}(S_m - \sigma - S) + p^c(S_m - \sigma) & \text{for } S > S_m - \sigma \end{cases} \quad [22]$$

where ϵ and σ are small parameters: $\epsilon = 1 \times 10^{-6}$ and $\sigma = 1 \times 10^{-3}$.

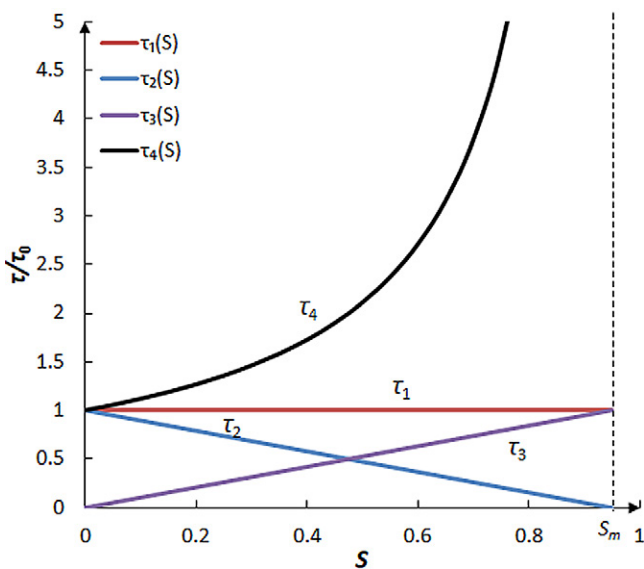


Fig. 5. Four different capillarity functions $\tau(S)$, defined in Table 2, for saturations S to the maximum saturation S_m .

Table 3. The values of the critical dynamic capillarity function λ_c for different capillarity functions $\tau(S)$ using parameters in Table 1.

Dynamic capillarity function	λ_c for $S_T = 0.33$
$\tau_1(S)$ (constant)	21.8
$\tau_2(S)$ (decreasing)	33.4
$\tau_3(S)$ (increasing)	62.8
$\tau_4(S)$ (increasing and non-integrable)	14.2

For numerical purposes, we truncate the column at a sufficiently large dimensionless length, where we prescribe the boundary condition $S = S_B$.

In solving the equations, we used the commercial software package COMSOL Multiphysics 5.0 (COMSOL, 2014). For the space–time discretization, we took $\Delta x = 0.01$ and $\Delta t_{\max} = 0.2$. This resulted in mesh-independent solutions.

Figures 6, 7, and 8 show typical profiles of the computed saturation. The observed behavior is explained by a traveling wave analysis given below. The dimensionless time in the figures was chosen so that the saturation front is sufficiently far from the top ($x = 0$) and from the truncated bottom ($x = L$).

From the figures, the following behavior can be observed:

1. Profiles move with fixed shape and speed through the column (see Fig. 6; traveling wave τ studied below).
2. When $\tau(S) = 1$ and λ is sufficiently small, there are no oscillations, which corresponds to observations by Cuesta et al. (2000), Nieber et al. (2005), and Sander et al. (2008). Overshoot increases with λ . When λ is large, the saturation reaches its maximal value S_m . The influence of the extended pressure Eq. [19] gives a saturation plateau where $S = S_m$ (see Fig. 7).
3. When τ is singular at $S = S_m$ as in Fig. 8, the plateau at $S = S_m$ disappears, no matter how large λ . This remarkable observation is explained below.

Traveling Wave Solution

Following up the numerical results, we consider here a special class of solutions of Eq. [17] and [19] having the form of traveling wave (TWs). They describe a situation where the saturation has reached a well-developed profile that moves through the column as a wave with a constant speed. Such solutions generally arise after longer times and are thus valid for long domains. These waves connect an upstream saturation (here equal to the inflow saturation S_T , determined by Eq. [18]) to a downstream saturation state (here equal to the initial saturation S_B), where $0 < S_B < S_T < S_m$.

Traveling wave solutions of Eq. [17] received considerable attention in the past. For instance, Cuesta et al. (2000) studied TWs in the interesting case of power law nonlinearities. They obtained existence, uniqueness, and non-monotonicity of solutions. Particular emphasis was on the behavior of solutions as $S_B \rightarrow 0$. Later, Nieber et al. (2005) numerically evaluated TW solutions in a more general

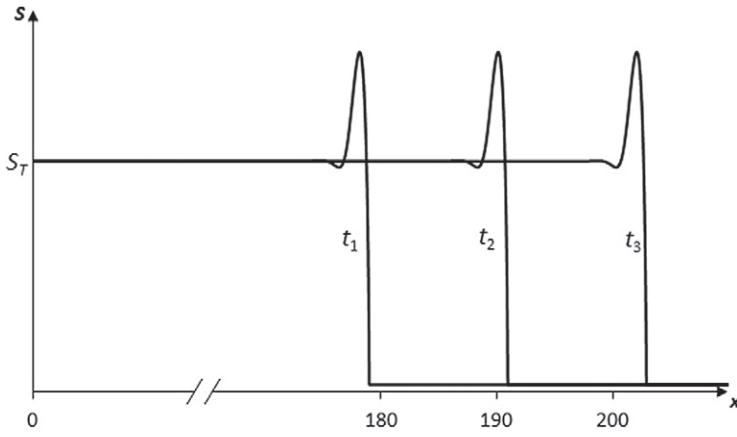


Fig. 6. Saturation profiles with capillarity coefficient $\tau(S) = 1$ and dimensionless capillarity coefficient $\lambda = 50$ at three different times $t_1 = 7500$, $t_2 = 8000$, and $t_3 = 8500$.

setting and investigated their stability. Recently, van Duijn et al. (2018) reported on analytical results concerning the dependence of TW solutions on the coefficient λ and the function $\tau(S)$ in Eq. [17b]. Here we essentially summarize their results. We will then interpret these findings in terms of their hydrological significance.

In mathematical terms, TWs are described by solutions of the form

$$S(x, t) = S(\eta) \quad \text{and} \quad u(x, t) = u(\eta) \quad [23]$$

where $\eta = x - ct$. The unknowns are the saturation profile $S(\eta)$, the pressure profile $u(\eta)$, and the wave (or propagation) speed c . They are obtained from the corresponding equations and boundary conditions. The boundary conditions for TWs are attained at $\eta = \pm\infty$ (i.e., $x = \pm\infty$) and are given by

$$\begin{aligned} [S(-\infty), u(-\infty)] &= [S_T, p^c(S_T)] \\ \text{and } [S(+\infty), u(+\infty)] &= [S_B, p^c(S_B)] \end{aligned} \quad [24]$$

Applying the traveling wave form to Eq. [17] and using the chain rule when differentiating, the ordinary differential equations are obtained:

$$-c \frac{dS}{d\eta} + \frac{d}{d\eta} \left[k(S) \left(\frac{du}{d\eta} + 1 \right) \right] = 0 \quad [25a]$$

$$u = p^c(S) + \lambda c \tau(S) \frac{dS}{d\eta} \quad [25b]$$

where $-\infty < \eta < \infty$.

Equation [25a] can be integrated to give

$$-cS + k(S) \left(\frac{du}{d\eta} + 1 \right) = C \quad [26]$$

where C is a constant of integration. We evaluate this equation at $\eta = \pm\infty$ and apply the boundary conditions of Eq. [24]. Because the pressure difference u attains constant (but different) values at $\eta = \pm\infty$, we must have $du/d\eta = 0$ when $\eta = \pm\infty$. Using this in Eq. [26] gives

$$\begin{cases} -cS_B + k(S_B) = C & (\eta = +\infty) \\ -cS_T + k(S_T) = C & (\eta = -\infty) \end{cases} \quad [27]$$

Solving these equations for c and C gives

$$c = \frac{k(S_T) - k(S_B)}{S_T - S_B} \quad [28]$$

$$C = \frac{k(S_B)S_T - k(S_T)S_B}{S_T - S_B} \quad [29]$$

Note that c is the well-known Rankine–Hugoniot speed (Renardy and Rogers, 2004).

Rearranging Eq. [25b] and substituting Eq. [28] and [29] into Eq. [26] yields the system of first-order equations

$$\frac{dS}{d\eta} = \frac{u - p^c(S)}{\lambda c \tau(S)} \quad [30a]$$

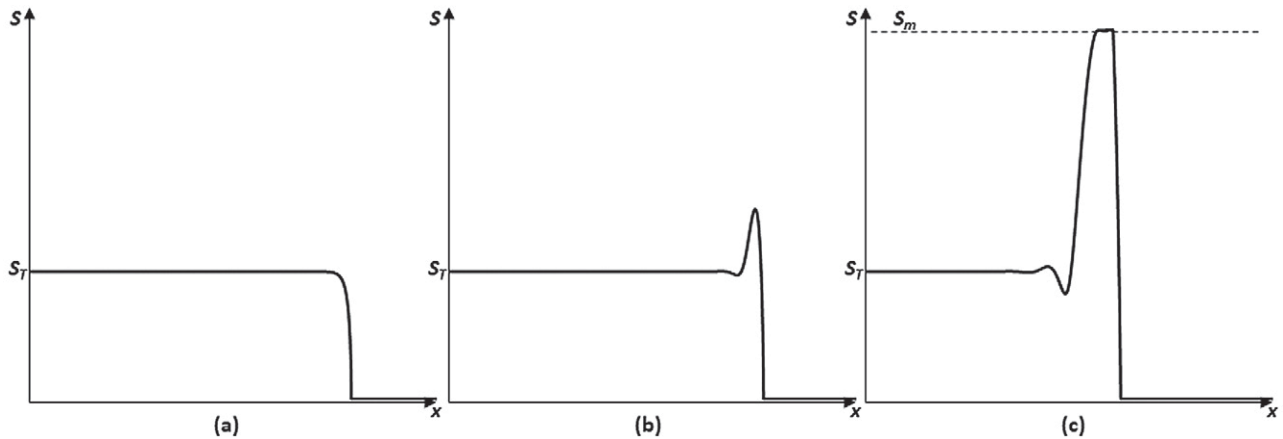


Fig. 7. Saturation profiles with capillarity coefficient $\tau(S) = 1$ at time $t = 8000$ for three different values of the dimensionless dynamic capillarity coefficient λ : (a) 10, (b) 50, and (c) 100.

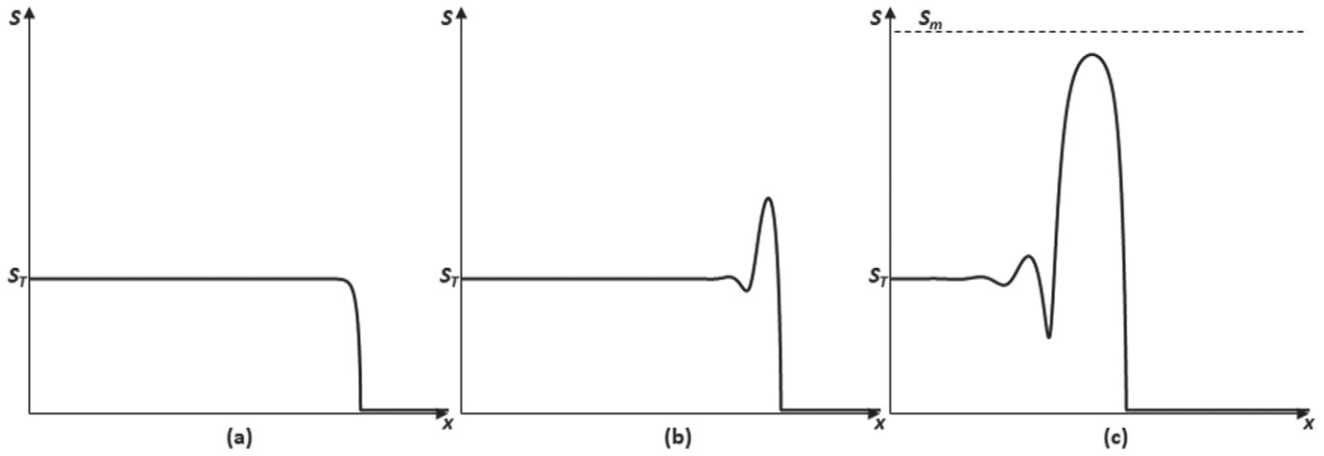


Fig. 8. Saturation profiles with capillarity coefficient $\tau(S) = 1/(1 - S/S_m)$ at time $t = 8000$ for three different values of dimensionless dynamic capillarity coefficient λ : (a) 10, (b) 50, and (c) 100.

$$\frac{d\mu}{d\eta} = G(S; S_B, S_T) \quad [30b]$$

where

$$G(S; S_B, S_T) = \frac{k(S_B) + c(S - S_B)}{k(S)} - 1 \quad [31]$$

for $0 < S \leq S_m$.

The function G is shown in Fig. 9. The linear function in G , $l(S) = k(S_B) + c(S - S_B)$, has two intersection points with the function $k(S)$, i.e., points $[S_B, k(S_B)]$ and $[S_T, k(S_T)]$. The permeability $k(S) < l(S)$ between the two points, whereas $k(S) > l(S)$ when $S < S_B$ or $S > S_T$. Therefore we have

$$G(S; S_B, S_T) \begin{cases} > 0 & \text{for } S_B < S < S_T \\ = 0 & \text{for } S = S_B, S_T \\ < 0 & \text{for } 0 < S < S_B, S_T < S \leq S_m \end{cases} \quad [32]$$

The two equilibrium points corresponding to S_B and S_T (when the right-hand sides of Eq. [30] vanish) are

$$E_B = [S_B, p^c(S_B)] \quad \text{and} \quad E_T = [S_T, p^c(S_T)] \quad [33]$$

These points correspond to the boundary condition Eq. [24].

A solution $[S(\eta), \mu(\eta)]$, with $-\infty < \eta < \infty$, will be represented as a trajectory in the $S-\mu$ plane. This trajectory connects the point E_T , as $\eta \rightarrow -\infty$, to the point E_B , as $\eta \rightarrow \infty$.

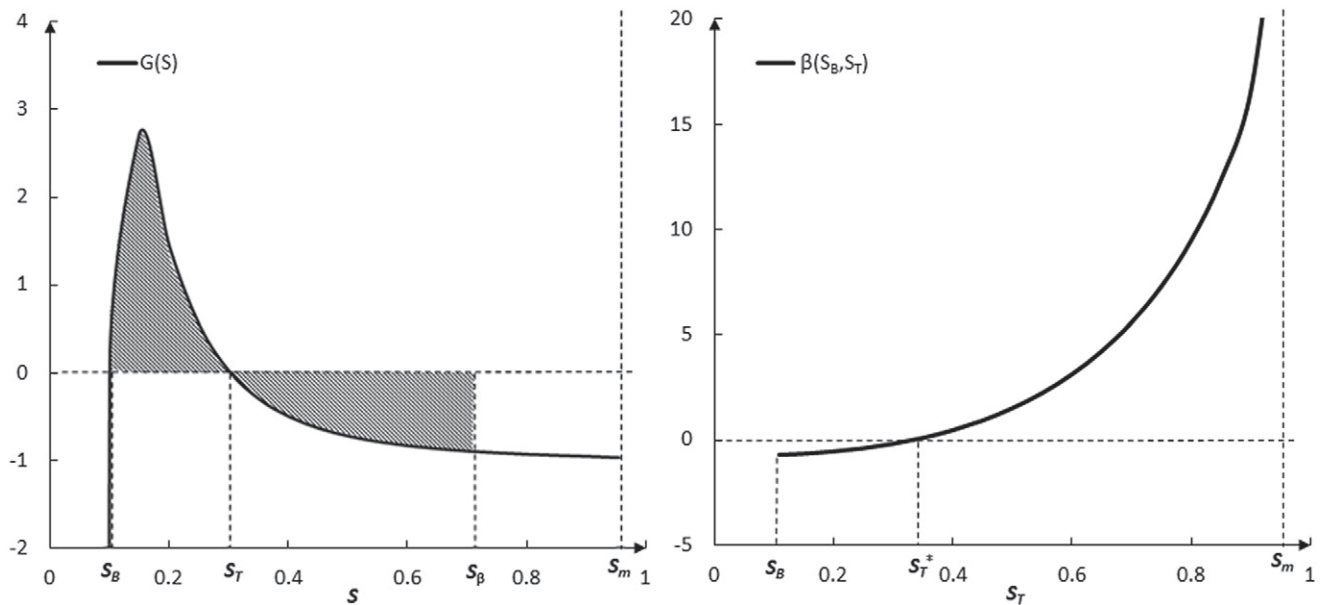


Fig. 9. Graph of the function $G(S; S_B, S_T)$, defined by Eq. [31], for a given $S_B < S_T < S_m$ where $S_B = 0.1$ and $S_T = 0.33$ and where the upper saturation S_β is indicated by the boundary of the gray region (left), and graph of the integral $\beta(S_B, S_T)$, defined by Eq. [35], as a function of S_T for $S_B = 0.1$ where the special saturation $S_T^* = S_T^*(S_B)$ is indicated and both S_β and $\beta(S_B, S_T)$ correspond to capillarity coefficient $\tau(S) = 1$ (right).

For the construction of a connecting trajectory (i.e., solution), it is important to know the nature of the equilibrium points. Linearizing the system of Eq. [30] at E_T and E_B and computing the eigenvalues of the resulting matrices produces the following (e.g., Cuesta et al., 2000):

E_B is a saddle (positive and negative eigenvalues) [34a]

E_T is $\begin{cases} \text{an unstable node when } \lambda < \lambda_c \\ \text{(positive real eigenvalues)} \\ \text{an unstable spiral when } \lambda > \lambda_c \\ \text{(complex eigenvalues with positive real part)} \end{cases}$ [34b]

The critical λ value is given by (e.g., Cuesta et al., 2000)

$$\lambda_c = -\frac{[p^{c'}(S_T)]^2}{4c\tau(S_T)G'(S_T; S_B, S_T)} \quad [35]$$

where primes denote differentiation with respect to S .

The characterization of the equilibrium points, including Eq. [35], was observed earlier by Nieber et al. (2005) and Sander et al. (2008).

Thus when $\lambda > \lambda_c$, TWs can leave S_T only in an oscillatory way, yielding solutions with overshoot in the original variables. When $\lambda < \lambda_c$, a trajectory can go (at least in theory) at most a finite number of times around the point E_T . In the computations, we observed always monotonic behavior when $\lambda < \lambda_c$.

Because E_B is a saddle, it is practically impossible to find a trajectory that reaches E_B as $\eta \rightarrow \infty$. For this reason, we reversed the direction of the trajectories by setting $\xi = -\eta$. In terms of ξ , the trajectory runs from E_B , with $\xi = -\infty$, to E_T , with $\xi = \infty$. Reversing the direction also changes the sign of the eigenvalues. Thus in terms of ξ , E_T is a stable spiral when $\lambda > \lambda_c$ and a stable node when $\lambda < \lambda_c$. To compute the reversed trajectory, the direction of the eigenvector corresponding to the positive eigenvalue at E_B ($\xi = -\infty$) is computed. Along this direction, a point is chosen sufficiently close to E_B as a starting point for the computation: i.e., as initial conditions for the system Eq. [30]. The reversed situation is sketched in Fig. 10.

According to Cuesta et al. (2000), van Duijn et al. (2018) proved the existence of a connecting trajectory (orbit) for each $\lambda > 0$ and for general functions $\tau(S)$. The qualitative properties of the corresponding saturation depend critically on the choice of S_B and S_T and on the dynamic capillarity coefficient $\lambda\tau(S)$. The main results are the following:

Let $0 < S_B < S_T < S_m$ and distinguish the cases (van Duijn et al., 2018)

$$\int_0^{S_m} \tau(S) dS < \infty \quad (\tau \text{ in Class A})$$

$$\int_0^{S_m} \tau(S) dS = \infty \quad (\tau \text{ in Class B})$$

A. For a given $\tau(S)$ in Class A, introduce the function (van Duijn et al., 2018)

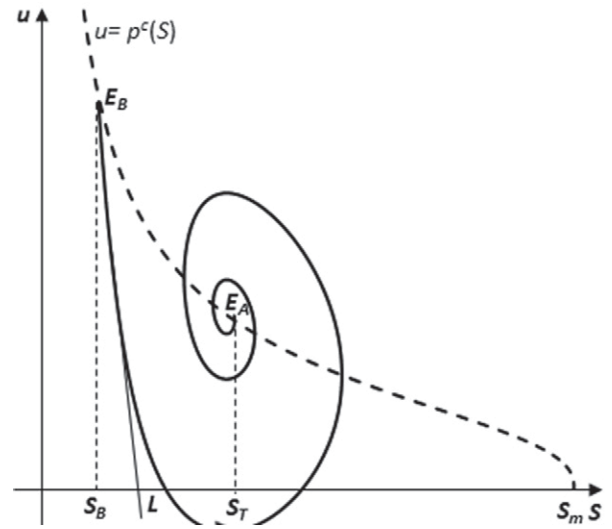


Fig. 10. Sketch of u - S trajectory in reversed direction $\xi = -\eta = ct - x$ when $\lambda > \lambda_c$. Line L coincides with the direction of the eigenvector corresponding to the positive eigenvalues at E_B . The arrow indicates the direction of increasing ξ .

$$\beta(S_B, S_T) = \int_{S_B}^{S_m} G(S; S_B, S_T) f(S) dS \quad [36]$$

and the saturation S_β , defined by (van Duijn et al., 2018)

$$\int_{S_B}^{S_\beta} G(S; S_B, S_T) f(S) dS = 0 \quad [37]$$

The proportion of the function G implies that for each fixed S_B , $\beta(S_B, S_T = S_B) < 0$

$$\beta(S_B, S_T = S_m) > 0$$

and $\beta(S_B, S_T)$ increases monotonically with S_T . Hence there exists a unique value of $S_T = S_T^*$, depending on S_B , such that $\beta(S_B, S_T) = 0$. Thus

$$\beta(S_B, S_T) < 0 \quad \text{for } S_T < S_T^*(S_B) \quad [38a]$$

$$\beta(S_B, S_T) > 0 \quad \text{for } S_T > S_T^*(S_B) \quad [38b]$$

Typical behavior of β is shown in Fig. 9.

Similarly, the saturation S_β depends on S_B and S_T as well. From Fig. 9, we can see that $S_T < S_\beta < S_m$, and $S_\beta \rightarrow S_B$ as $S_T \rightarrow S_B$, and $S_\beta \rightarrow S_m$ as $S_T \rightarrow S_T^*(S_B)$.

Thus the following holds:

The maximal saturation overshoot increases with the capillarity constant λ such that:

- a1. If S_B and S_T are such that $\beta(S_B, S_T) < 0$, i.e., $S_T < S_T^*(S_B)$, then the saturation overshoot remains bounded away from the maximal value S_m no matter how large λ . More precisely, if $S_T < S_T^*(S_B)$, then $S(\eta) < S_\beta < S_m$ for $\eta \in \mathbb{R}$ and for all $\lambda > 0$.

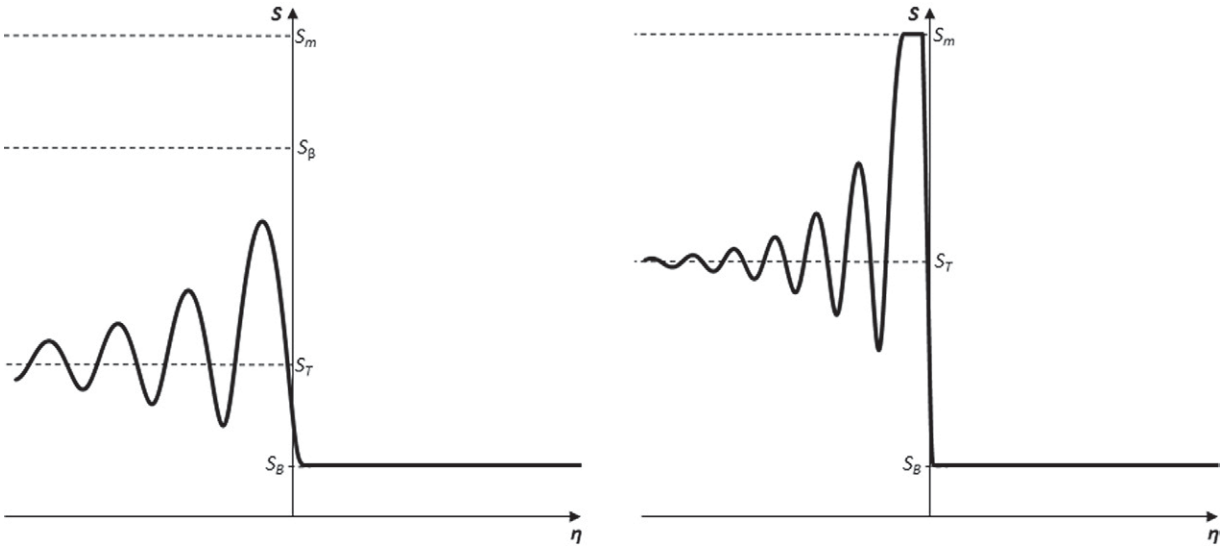


Fig. 11. Sketch of saturation profiles: $\beta(S_B, S_T) < 0$ and $S(\eta) < S_B < S_m$, for all $\eta \in R$ no matter how large $\lambda > 0$ (left); and $\beta(S_B, S_T) > 0$ and there exists a saturation overshoot with a plateau at $S = S_m$ when λ is sufficiently large (i.e., $\lambda > \lambda^*$) (right). The profiles are normalized such that $S(0) = (S_B + S_T)/2$.

- a2. If S_B and S_T are such that $\beta(S_B, S_T) > 0$, i.e., $S_T > S_T^*(S_B)$, then there exists a second critical value of λ , $\lambda^* > \lambda_c$, such that if $\lambda < \lambda^*$, the saturation does not reach the maximum value S_m , and $S(\eta) < S_m$ for $\eta \in R$; if $\lambda > \lambda^*$, the saturation has an overshoot with a plateau at the maximal value S_m .

Both Cases a1 and a2 are sketched in Fig. 11.

- B. For a given $\tau(S)$ in Class B, the following holds. Again, the maximal saturation overshoot increases when the capillarity constant λ increases, but $S(\eta) < S_B < S_m$ for $\eta \in R$ and for all $\lambda > 0$. Here S_B is again given by Eq. [37].

This inequality may come as a surprise because $\tau(S)$ in Class B means that $\tau(S)$ has a singularity at $S = S_m$. Thus one expects a strong effect of the dynamic capillarity term at $S = S_m$. However, for the function $\beta(S_B, S_T)$, with $\tau(S)$ from Class B, $\beta(S_B, S_T) = -\infty$ for each $S_B < S_T < S_m$.

So loosely speaking, one is always in the situation described by Case a1 for any $S_T < S_m$.

Results and Discussion

Growth of Saturation Overshoot

As explained above, the growth of saturation overshoot was influenced by both the functional form of $\tau(S)$ and the value of λ . We solved the full equations accounting for various combinations of different λ values and $\tau(S)$ forms. The computed saturation profiles at three different time intervals are shown in Fig. 12. Figures 12a and 12b show the solutions obtained with the functional form $\tau_1(S)$ and values $\lambda = 50$ and $\lambda = 100$, respectively. The saturation overshoot obtained with $\lambda = 50$ reaches a fixed shape at $t_1 = 1000$, while the overshoot obtained with $\lambda = 100$ still grows slightly at $t_3 = 3000$. Figure 12c shows the solution obtained with the functional form $\tau_4(S)$ and $\lambda = 100$. The overshoot is still far from the fixed shape at $t_3 = 3000$. These behaviors indicate that the valid

distance of the traveling wave solution varies depending on the functional forms and values of the dynamic capillarity coefficient.

Influence of Different Expressions for the Capillarity Coefficient

The traveling wave Eq. [30–32] were solved numerically using MATLAB (2016). As shown by Eq. [35], the critical value λ_c depends on the functional form of $\tau(S)$. Corresponding to the expressions in Table 2, we have the values of λ_c listed in Table 3 for fixed $S_T = 0.33$. The resulting $u-S$ trajectories are shown in Fig. 13. The inset shows an enlargement of the curves near S_T . The computations are done for different values of λ . The primary imbibition curve under quasi-static conditions is shown as the dotted line, while the solid lines with different colors represent $S-u$ curves for different values of λ . Values $\lambda = 10$ (which is less than λ_c ; see Table 3), 50, and 200 (which are both larger than λ_c) were combined with $\tau_1(S)$, $\tau_2(S)$, and $\tau_4(S)$. For $\tau_3(S)$, however, these values do not result in any distinct overshoot behavior. Therefore we chose λ values of 1000 and 8000 to show distinctly different saturation overshoot behaviors. The results obtained for $\tau_1(S)$ are shown in Fig. 13a. Note that the solution is monotonic when $\lambda < \lambda_c$. For $\lambda > \lambda_c$, however, there exists a saturation overshoot (being larger for larger λ values) along with small saturation oscillations. For the largest value $\lambda = 100$, the maximum saturation of S_m is reached, and the solution follows the extension of the capillary pressure (Eq. [22]). Similarly, for the decreasing integrable $\tau_2(S)$ and increasing integrable $\tau_3(S)$, the saturation reaches S_m for larger λ values (see Fig. 13b and 13c). However, in the case of the non-integrable increasing $\tau_4(S)$, the saturation has a smooth plateau when close to S_m , but the saturation always remains just below S_m .

Correspondence with Experimental Observations

We next perform two sets of calculations using the parameters reported by DiCarlo (2004) and Fritz (2012). Their experimental

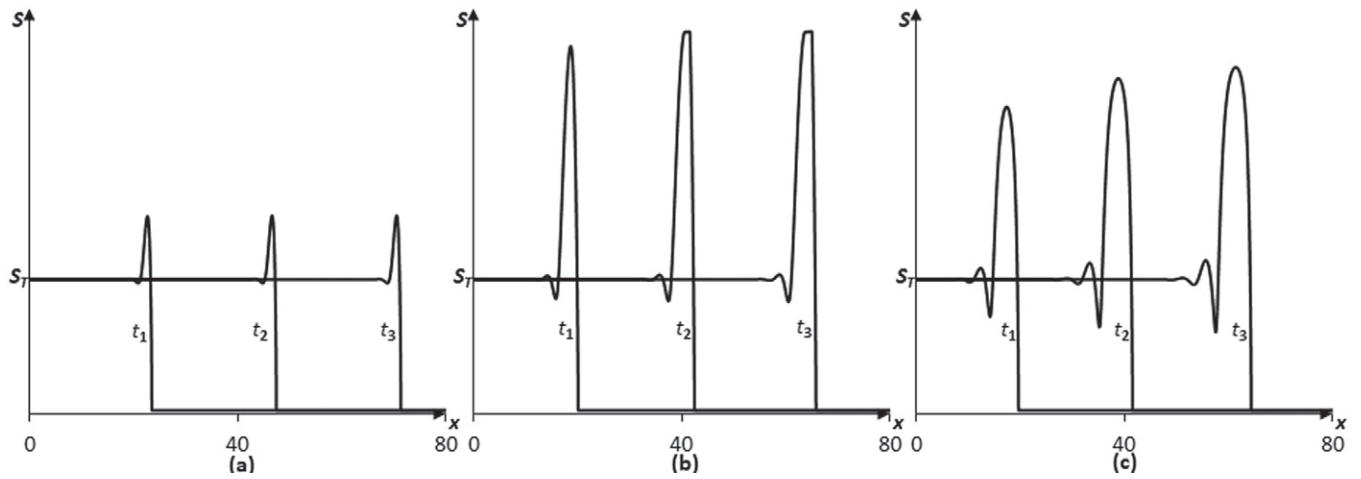


Fig. 12. Saturation profiles at $t_1 = 1000$, $t_2 = 2000$, and $t_3 = 3000$: (a) capillarity coefficient $\tau(S) = 1$, dimensionless capillarity coefficient $\lambda = 50$; (b) $\tau(S) = 1$, $\lambda = 100$; (c) $\tau(S) = 1/(1 - S/S_m)$, $\lambda = 100$.

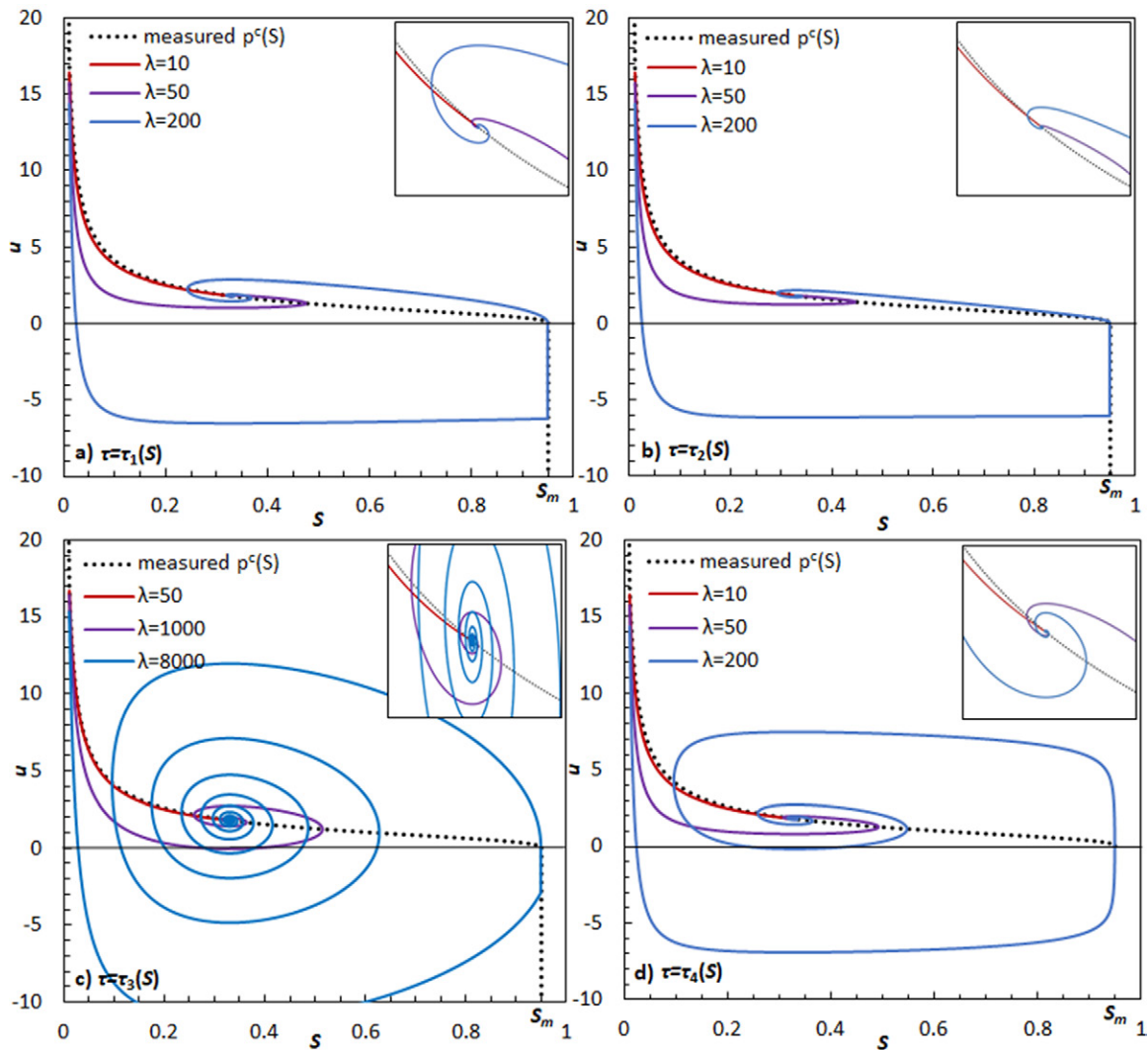


Fig. 13. Saturation–pressure difference curves for different forms of the capillarity coefficient $\tau(S)$: (a) constant $\tau_1(S)$; (b) decreasing $\tau_2(S)$; (c) increasing $\tau_3(S)$; and (d) non-integrable increasing $\tau_4(S)$.

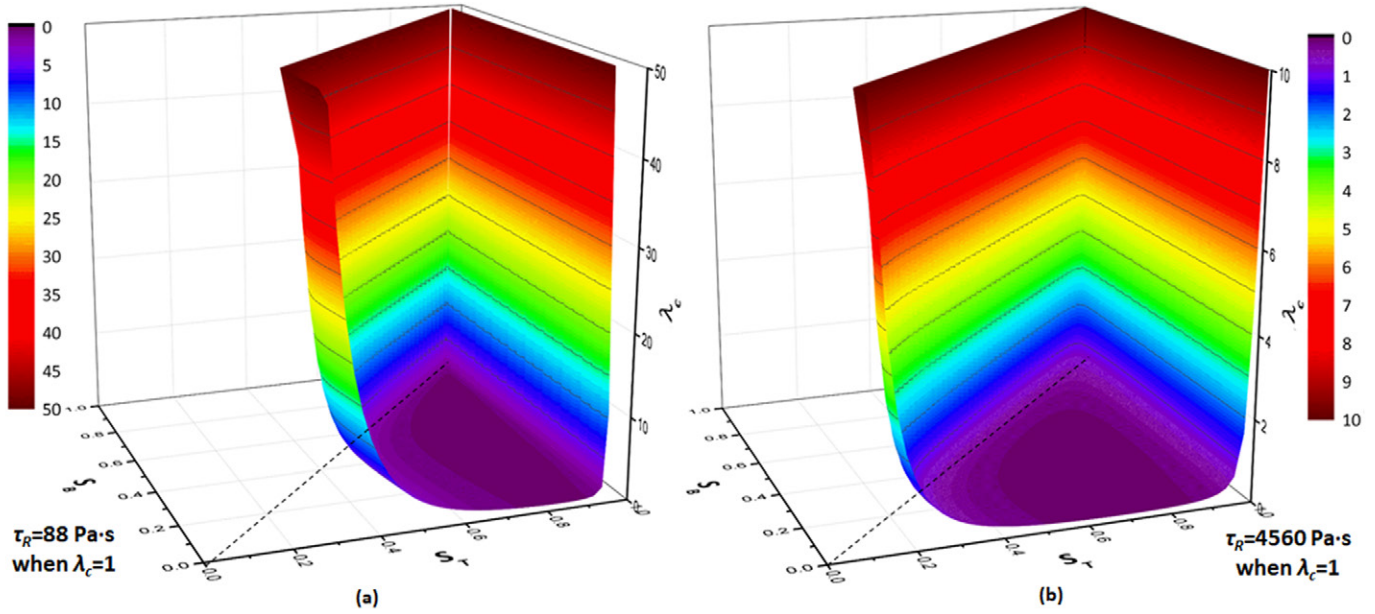


Fig. 14. The S_T - S_B - λ_c surfaces obtained with the experimental parameters reported by (a) Fritz (2012) and (b) DiCarlo (2004).

results can be found in Fig. 1 and 2. As explained above, the functional forms of $\tau(S)$ influence the traveling wave behavior. Here we show only the results of the cases obtained with constant τ , i.e., the function $\tau_1(S)$.

As shown by Eq. [35], the critical value λ_c depends on the values of S_T and S_B . Obviously, there exists a surface to show the relationships among λ_c , S_T , and S_B . Figures 14a and 14b show the S_T - S_B - λ_c surfaces for the two experiments. The value of S_B is always smaller or equal to S_T , so that the surfaces are located in

the region $S_B \leq S_T$. As can be seen, the shapes of surfaces obtained with the two sets of data are quite similar.

There exist three characteristics for the S_T - S_B - λ_c relationship:

1. The values of λ_c increase dramatically when $S_B \rightarrow S_T$ and/or $S_T \rightarrow S_m$, approaching infinity.
2. The values of λ_c increase with decreasing S_T values.
3. However, there is no distinct correlation between λ_c and S_B when S_B is much smaller than S_T .

We can interpret these findings into experimental behaviors in the following:

1. When the value of initial saturation (S_B) is quite close to the inlet saturation value (S_T), there exists no saturation overshoot (i.e., λ_c goes to the infinity). Also, the saturation profile is monotonic when the inflow rate is close to the saturated conductivity (see the curve for the 11.8 cm/min experiment in Fig. 1).
2. It is more probable to obtain saturation overshoot for larger inflow rates (means λ_c will be smaller). This explains the observation in DiCarlo's work that the saturation overshoot is larger for larger inflow rates.

Next, we calculate the values of S_T^* and S_β for the two experiments. The results are shown in Table 4.

Based on the traveling wave solution, the saturation is always smaller than S_β when $S_T < S_T^*$, while the saturation approaches S_m when $S_T \geq S_T^*$ (see Cases a1 and a2 and Fig. 11).

In DiCarlo's work, the values of S_β can be calculated for the two smallest inflow rates. The values are consistent with the maximum saturation value of overshoot. For the large inflow rates, the traveling wave analysis indicates that the saturation overshoot is close to S_m . As explained, the valid distance of the

Table 4. The calculated values of S_β (Eq. [37]) and S_T^* (Eq. [38]) based on the parameters reported by DiCarlo (2004) and Fritz (2012).

Experiments†			Traveling wave‡			
Flow rate	S_{inlet}	$S_{overshoot}$	S_T	S_T^*	S_B	S_β
cm/min						
DiCarlo (2004)						
8×10^{-4}	0.17	–	0.04	0.15	0.01	0.09
0.0079	0.17	0.28	0.08		0.01	0.35
0.079	0.26	0.67	0.18		0.01	–
0.79	0.38	0.82	0.40		0.01	–
7.9	0.78	0.92	0.84		0.01	–
11.8	0.96	–	0.95		0.01	–
Fritz (2012)						
0.26	0.33	0.74	0.33	0.09	0.01	–
0.26	0.33	0.50	0.33	0.17	0.03	–
0.26	0.33	–	0.33	0.34	0.10	0.89

† S_{inlet} , saturation at the inlet in the experiments; $S_{overshoot}$, maximum saturation of overshoot in the experiments.

‡ S_T , inflow saturation; S_B , initial saturation.

traveling wave indeed varies for different heights of saturation overshoot. Therefore, it is reasonable that the higher overshoot still grows to reach S_m .

Including hysteresis in capillary pressure and relative permeability has a significant impact on numerical solutions of full equations. Detailed numerical simulations of full equations including capillary and permeability hysteresis for constant τ can be found in Zhuang (2017). Theoretically, there are only partial results for the case of combined hysteresis in the relative permeability and the capillary pressure. Having only hysteresis in capillary pressure does not affect the overshoot in essence, since the system will be in imbibition mode. For a constant τ value, traveling wave analysis including capillary hysteresis has been reported by Mitra and van Duijn (2018).

Summary and Conclusions

We performed traveling wave analysis of water infiltration into relatively dry soil. Based on the literature overview, we considered four different expressions to specify the dependence of the dynamic capillarity coefficient on the saturation: constant $\tau_1(S)$, decreasing $\tau_2(S)$, increasing $\tau_3(S)$, and non-integrable increasing $\tau_4(S)$.

The analytical results have shown that there exists a critical value λ_c for the dynamic capillarity coefficient; there are no oscillations when τ is smaller than the critical value λ_c . This value depends on the functional forms of τ , the inlet saturation S_T , and the initial saturation S_B . There exist explicit upper bounds of the saturation overshoot. We have extended the definition of capillary pressure at the maximum saturation to prevent saturation from exceeding unity. This may result in a saturation plateau for large τ values. However, the plateau disappears when $\tau(S)$ is singular at the maximum saturation [e.g., for non-integrable functions such as $\tau_4(S)$].

We have compared these findings with experimental observations. We calculated the $S_T - S_B - \lambda_c$ relationship and upper bounds of overshoot using the parameters reported by DiCarlo (2004) and Fritz (2012). The value of λ_c was found to increase dramatically when S_B is close to S_T , and/or S_T is close to the maximum water saturation, approaching infinity. The values of λ_c increase when S_T values decrease. These findings are consistent with experimental observations. This is the first time that such a study of traveling wave analysis of this problem has been performed.

In this study, we have disregarded the hysteresis in the capillary pressure and the relative permeability; only the primary imbibition curves for capillary pressure and relative permeability were used. In a full analysis of the experiments, hysteretic effects must be included as well.

Acknowledgments

We would like to thank M.Th. van Genuchten for his comments on the manuscript. This work was carried out in collaboration with the Darcy Centre. S.M. Hassanizadeh has received funding from the European Research Council under the European Union's Seventh Framework Program (FP/2007-2013)/ERC Grant Agreement no. 341225. We would like to thank two anonymous reviewers for providing comments to the manuscript.

References

- Baker, R.S., and D. Hillel. 1990. Laboratory tests of a theory of fingering during infiltration into layered soils. *Soil Sci. Soc. Am. J.* 54:20–30. doi:10.2136/sssaj1990.03615995005400010004x
- Berentsen, C.W., S.M. Hassanizadeh, A. Bezuijen, and O. Oung. 2006. Modelling of two-phase flow in porous media including non-equilibrium capillary pressure effects. In: P.J. Binning et al., editors, *Proceedings of the XVI International Conference on Computational methods in Water Resources*, Copenhagen. 18–22 June 2006. Tech. Univ. of Denmark, Kongens Lyngby.
- Bottero, S., S.M. Hassanizadeh, P.J. Kleingeld, and A. Bezuijen. 2006. Experimental study of dynamic capillary pressure effect in two-phase flow in porous media. In: P.J. Binning et al., editors, *Proceedings of the XVI International Conference on Computational methods in Water Resources*, Copenhagen. 18–22 June 2006. Tech. Univ. of Denmark, Kongens Lyngby.
- Bottero, S., S.M. Hassanizadeh, P.J. Kleingeld, and T.J. Heimovaara. 2011. Nonequilibrium capillarity effects in two-phase flow through porous media at different scales. *Water Resour. Res.* 47:W10505. doi:10.1029/2011WR010887
- Camps-Roach, G., D.M. O'Carroll, T.A. Newson, T. Sakaki, and T.H. Illangasekare. 2010. Experimental investigation of dynamic effects in capillary pressure: Grain size dependency and upscaling. *Water Resour. Res.* 44:W08544. doi:10.1029/2009WR008881
- Cao, X., and I.S. Pop. 2016. Degenerate two-phase porous media flow model with dynamic capillarity. *J. Differ. Equations* 260:2418–2456. doi:10.1016/j.jde.2015.10.008
- Chapwanya, M., and J.M. Stockie. 2010. Numerical simulations of gravity-driven fingering in unsaturated porous media using a nonequilibrium model. *Water Resour. Res.* 46:W09534. doi:10.1029/2009WR008583
- COMSOL. 2014. *COMSOL Multiphysics 5.0*. COMSOL Inc., Burlington, MA.
- Cuesta, C., and J. Hulshof. 2003. A model problem for groundwater flow with dynamic capillary pressure: Stability of travelling waves. *Nonlinear Anal.* 52:1199–1218. doi:10.1016/S0362-546X(02)00160-8
- Cuesta, C., C.J. van Duijn, and J. Hulshof. 2000. Infiltration in porous media with dynamic capillary pressure: Travelling waves. *Eur. J. Appl. Math.* 11:381–397. doi:10.1017/S0956792599004210
- Dahle, H.K., M.A. Celia, and S.M. Hassanizadeh. 2005. Bundle-of-tubes model for calculating dynamic effects in the capillary-pressure-saturation relationship. *Transp. Porous Media* 58:5–22. doi:10.1007/s11242-004-5466-4
- Das, D.B., and M. Mirzaei. 2012. Dynamic effects in capillary pressure relationships for two-phase flow in porous media: Experiments and numerical analyses. *AIChE J.* 58:3891–3903.
- Diamantopoulos, E., and W. Durner. 2012. Dynamic nonequilibrium of water flow in porous media: A review. *Vadose Zone J.* 11(3). doi:10.2136/vzj2011.0197
- DiCarlo, D.A. 2004. Experimental measurements of saturation overshoot on infiltration. *Water Resour. Res.* 40:W04215. doi:10.1029/2003WR002670
- DiCarlo, D.A. 2007. Capillary pressure overshoot as a function of imbibition flux and initial water content. *Water Resour. Res.* 43:W08402. doi:10.1029/2006WR005550
- DiCarlo, D.A. 2013. Stability of gravity-driven multiphase flow in porous media: 40 years of advancements. *Water Resour. Res.* 49:4531–4544. doi:10.1002/wrcr.20359
- Egorov, A.G., R.Z. Dautov, J.L. Nieber, and A.Y. Sheshukov. 2002. Stability analysis of traveling wave solution for gravity-driven flow. *Dev. Water Sci.* 47:121–128. doi:10.1016/S0167-5648(02)80053-3
- Elzeftawy, A., and R.S. Mansell. 1975. Hydraulic conductivity calculations for unsaturated steady-state and transient-state flow in sand. *Soil Sci. Soc. Am. Proc.* 39:599–603.
- Fritz, S. 2012. Experimental investigations of water infiltration into unsaturated soil: Analysis of dynamic capillarity effects. M.S. thesis. Stuttgart Univ., Stuttgart, Germany.
- Fučík, R., J. Mikyška, S. Toshihiro, M. Beneš, and T.H. Illangasekare. 2010. Significance of dynamic effect in capillarity during drainage experiments in layered porous media. *Vadose Zone J.* 9:697–708. doi:10.2136/vzj2009.0106
- Gielen, T.W.J. 2007. Dynamic effect in two-phase flow in porous media: A pore-scale network approach. Ph.D. diss. Technische Univ. Delft, Delft, the Netherlands.

- Goel, G., and D.M. O'Carroll. 2011. Experimental investigation of nonequilibrium capillarity effects: Fluid viscosity effects. *Water Resour. Res.* 47:W09507. doi:10.1029/2010WR009861
- Hassanizadeh, S.M., M.A. Celia, and H.K. Dahle. 2002. Dynamic effect in the capillary pressure–saturation relationship and its impacts on unsaturated flow. *Vadose Zone J.* 1:38–57. doi:10.2136/vzj2002.3800
- Hassanizadeh, S.M., and W.G. Gray. 1990. Mechanics and thermodynamics of multiphase flow in porous media including interphase boundaries. *Adv. Water Resour.* 13:169–186. doi:10.1016/0309-1708(90)90040-B
- Hassanizadeh, S.M., and W.G. Gray. 1993. Thermodynamic basis of capillary pressure in porous media. *Water Resour. Res.* 29:3389–3405. doi:10.1029/93WR01495
- Hassanizadeh, S.M., O. Oung, and S. Manthey. 2004. Laboratory experiments and simulations on the significance of non-equilibrium effect in the capillary pressure–saturation relationship. In: T. Schanz, editor, *Unsaturated soil: Experimental studies. Proceedings of the International Conference "From Experimental Evidence towards Numerical Modeling of Unsaturated Soils"*, Weimar, Germany, 18–19 Sept. 2003. Springer Proc. Phys. 93. Springer, Berlin. p. 3–14.
- Joekar-Niasar, V., and S.M. Hassanizadeh. 2011. Effect of fluids properties on non-equilibrium capillarity effects: Dynamic pore-network modeling. *Int. J. Multiphase Flow* 37:198–214. doi:10.1016/j.ijmultiphaseflow.2010.09.007
- Joekar-Niasar, V., and S.M. Hassanizadeh. 2012. Analysis of fundamentals of two-phase flow in porous media using dynamic pore-network models: A review. *Crit. Rev. Environ. Sci. Technol.* 42:1895–1976. doi:10.1080/10643389.2011.574101
- Joekar-Niasar, V., S.M. Hassanizadeh, and H.K. Dahle. 2010. Non-equilibrium effects in capillarity and interfacial area in two-phase flow: Dynamic pore-network modelling. *J. Fluid Mech.* 655:38–71. doi:10.1017/S0022112010000704
- Kalaydjian, F. 1987. A macroscopic description of multiphase flow in porous media involving spacetime evolution of fluid/fluid interface. *Transp. Porous Media* 2:537–552. doi:10.1007/BF00192154
- Manthey, S., S.M. Hassanizadeh, and R. Helmig. 2005. Macro-scale dynamic effects in homogeneous and heterogeneous porous media. *Transp. Porous Media* 58:121–145. doi:10.1007/s11242-004-5472-6
- MATLAB. 2016. MATLAB R2016a. MathWorks, Natick, MA.
- Mirzaei, M., and D.B. Das. 2007. Dynamic effects in capillary pressure–saturation relationships for two-phase flow in 3D porous media: Implications of micro-heterogeneities. *Chem. Eng. Sci.* 62:1927–1947. doi:10.1016/j.ces.2006.12.039
- Mitra, K., and C.J. van Duijn. 2018. Wetting fronts in unsaturated porous media: The combined case of hysteresis and dynamic capillary. UHasselt Comput. Math. Preprint UP-18-03. Hasselt Univ., Hasselt, Belgium.
- Nieber, J.L., R.Z. Dautov, A.G. Egorov, and A.Y. Sheshukov. 2005. Dynamic capillary pressure mechanism for instability in gravity-driven flows: Review and extension to very dry conditions. *Transp. Porous Media* 58:147–172. doi:10.1007/s11242-004-5473-5
- O'Carroll, D.M., K.G. Mumford, L.M. Abriola, and J.I. Gerhard. 2010. Influence of wettability variations on dynamic effects in capillary pressure. *Water Resour. Res.* 46:W08505. doi:10.1029/2009WR008712
- O'Carroll, D.M., T.J. Phelan, and L.M. Abriola. 2005. Exploring dynamic effects in capillary pressure in multistep outflow experiments. *Water Resour. Res.* 41:W11419. doi:10.1029/2005WR004010
- Oung, O., S.M. Hassanizadeh, and A. Bezuijzen. 2005. Two-phase flow experiments in a geocentrifuge and the significance of dynamic capillary pressure effect. *J. Porous Media* 8:247–257. doi:10.1615/JPorMedia.v8.i3.10
- Rätz, A., and B. Schweizer. 2014. Hysteresis models and gravity fingering in porous media. *Z. Angew. Math. Mech.* 94:645–654. doi:10.1002/zamm.201200052
- Renardy, M., and R.C. Rogers. 2004. An introduction to partial differential equations. 2nd ed. *Texts Appl. Math.* 13. Springer, New York.
- Sakaki, T., D.M. O'Carroll, and T.H. Illangasekare. 2010. Direct quantification of dynamic effects in capillary pressure for drainage–wetting cycles. *Vadose Zone J.* 9:424–437. doi:10.2136/vzj2009.0105
- Sander, G.C., O.J. Glidewell, and J. Norbury. 2008. Dynamic capillary pressure, hysteresis and gravity-driven fingering in porous media. *J. Phys. Conf. Ser.* 138:012023. doi:10.1088/1742-6596/138/1/012023
- Smiles, D.E., G. Vachaud, and M. Vauclin. 1971. A test of the uniqueness of the soil moisture characteristic during transient, nonhysteretic flow of water in a rigid soil. *Soil Sci. Soc. Am. J.* 35:534–539. doi:10.2136/sssaj1971.03615995003500040018x
- Stauffer, F. 1978. Time dependence of the relations between capillary pressure, water content and conductivity during drainage of porous media. Paper presented at: IAHR symposium on scale effects in porous media, Thessaloniki, Greece. 29 Aug.–1 Sept. 1978. p. 3–35.
- Stonestrom, D.A., and K.C. Akstin. 1994. Nonmonotonic matric pressure histories during constant flux infiltration into homogeneous profiles. *Water Resour. Res.* 30:81–91.
- Topp, G., and A. Peters. 1967. Comparison of water content–pressure head data obtained by equilibrium, steady-state, and unsteady-state methods. *Soil Sci. Soc. Am. J.* 31:312–314. doi:10.2136/sssaj1967.03615995003100030009x
- Vachaud, G., and J. Thony. 1971. Hysteresis during infiltration and redistribution in a soil column at different initial water contents. *Water Resour. Res.* 7:111–127. doi:10.1029/WR007i001p00111
- van Duijn, C.J., Y. Fan, L.A. Peletier, and I.S. Pop. 2013. Travelling wave solutions for degenerate pseudo-parabolic equations modelling two-phase flow in porous media. *Nonlinear Anal. Real World Appl.* 14:1361–1383. doi:10.1016/j.nonrwa.2012.10.002
- van Duijn, C.J., K. Mitra, and I.S. Pop. 2018. Travelling wave solutions for the Richards equation incorporating non-equilibrium effects in the capillary pressure. *Nonlinear Anal. Real World Appl.* 41:232–268. doi:10.1016/j.nonrwa.2017.10.015
- van Duijn, C.J., L.A. Peletier, and I.S. Pop. 2007. A new class of entropy solutions of the Buckley–Leverett equation. *SIAM J. Math. Anal.* 39:507–536. doi:10.1137/05064518X
- van Duijn, C.J., G.J.M. Pieters, and P.A.C. Raats. 2004. Steady flows in unsaturated soils are stable. *Transp. Porous Media* 57:215–244. doi:10.1023/B:TIPM.0000038250.72364.20
- van Genuchten, M.Th. 1980. A closed-form equation for predicting the hydraulic conductivity of unsaturated soils. *Soil Sci. Soc. Am. J.* 44:892–898.
- Wang, Z., W.A. Jury, A. Tuli, and D.-J. Kim. 2004. Unstable flow during redistribution. *Vadose Zone J.* 3:549–559.
- Wildenschild, D., J.W. Hopmans, and J. Šimůnek. 2001. Flow rate dependence of soil hydraulic characteristics. *Soil Sci. Soc. Am. J.* 65:35–48. doi:10.2136/sssaj2001.65135x
- Xiong, Y. 2014. Flow of water in porous media with saturation overshoot: A review. *J. Hydrol.* 510:353–362. doi:10.1016/j.jhydrol.2013.12.043
- Zhang, H., and P.A. Zegeling. 2017. A numerical study of two-phase flow with dynamic capillary pressure using an adaptive moving mesh method. *J. Comput. Phys.* 345:510–527. doi:10.1016/j.jcp.2017.05.041
- Zhuang, L. 2017. Advanced theories of water redistribution and infiltration in porous media: Experimental studies and modeling. Ph.D. diss. Utrecht Univ., Utrecht, the Netherlands.